

# Copper-catalyzed asymmetric 1,3-dipolar cycloaddition of azomethine ylides with $\beta$ -trifluoromethyl-substituted alkenyl heteroarenes

Xiang Cheng<sup>1,2†</sup>, Xin Chang<sup>1,2†</sup>, Yuhong Yang<sup>3†</sup>, Zongpeng Zhang<sup>1</sup>, Jing Li<sup>1</sup>, Yipu Li<sup>1</sup>, Wenxiao Zhao<sup>1</sup>, Lung Wa Chung<sup>3\*</sup>, Huailong Teng<sup>4\*</sup>, Xiu-Qin Dong<sup>1\*</sup> & Chun-Jiang Wang<sup>1,2\*</sup>

<sup>1</sup>College of Chemistry and Molecular Sciences, Wuhan University, Wuhan 430072, China;

<sup>2</sup>State Key Laboratory of Organometallic Chemistry, Shanghai Institute of Organic Chemistry, Shanghai 230021, China;

<sup>3</sup>Shenzhen Grubbs Institute, Department of Chemistry and Guangdong Provincial Key Laboratory of Catalysis, Southern University of Science and Technology, Shenzhen 518055, China;

<sup>4</sup>College of Science, Huazhong Agricultural University, Wuhan 430070, China

Received June 1, 2023; accepted June 30, 2023; published online August 23, 2023

Copper-catalyzed asymmetric 1,3-dipolar cycloaddition of azomethine ylides and  $\beta$ -trifluoromethyl-substituted alkenyl heteroarenes was developed for the first time. A wide range of enantioenriched pyrrolidines containing both heteroarenes and trifluoromethyl group with multiple stereogenic centers could be readily accessible by this method with good to high yields and excellent levels of both stereo- and regioselectivity (up to 99% yield, >20:1 rr, >20:1 dr, and up to 95% ee). Notably, substrate-controlled umpolung-type dipolar cycloaddition was also disclosed in this protocol to achieve regiodivergent synthesis with  $\alpha$ -aryl substituted aldimine esters as the dipole precursors. Systematic DFT studies were conducted to explore the origin of the stereo- and regioselectivity of this 1,3-dipolar cycloaddition, and suggest that copper(II) salt utilized in this catalytic system could be reduced *in-situ* to the active copper(I) species and might be responsible for the observed high stereo- and regioselectivity.

**asymmetric catalysis, 1, 3-dipolar cycloaddition, chiral pyrrolidines, heteroarene, trifluoromethyl group**

**Citation:** Cheng X, Chang X, Yang Y, Zhang Z, Li J, Li Y, Zhao W, Chung LW, Teng H, Dong XQ, Wang CJ. Copper-catalyzed asymmetric 1,3-dipolar cycloaddition of azomethine ylides with  $\beta$ -trifluoromethyl-substituted alkenyl heteroarenes. *Sci China Chem*, 2023, 66: 3193–3204, <https://doi.org/10.1007/s11426-023-1683-9>

## 1 Introduction

Chiral pyrrolidines containing multiple stereogenic centers as valuable scaffolds are not only commonly found in many biologically active natural products, pharmaceuticals and agricultural chemicals, but they also work as chiral organo-catalysts, ligands and useful building blocks in asymmetric

synthesis [1–14]. In addition, heteroarenes (*e.g.*, benzoxazolyl, benzothiazolyl, pyridines, and others) [15–19] and trifluoromethylated organic compounds [20–28] are fascinating functional groups in biologically active compounds, agrochemicals, pharmaceuticals, and functional materials. The introduction of trifluoromethyl group into molecules always has a profound effect on the parent molecules, including the alteration of physicochemical and biological properties [23,29–32]. Therefore, considerable attention has been attracted in the last decades. Considering the importance of these versatile building units, it is extremely

†These authors contributed equally to this work.

\*Corresponding authors (email: [oscarchung@sustech.edu.cn](mailto:oscarchung@sustech.edu.cn); [thlong@mail.hzau.edu.cn](mailto:thlong@mail.hzau.edu.cn); [xiuqindong@whu.edu.cn](mailto:xiuqindong@whu.edu.cn); [cjwang@whu.edu.cn](mailto:cjwang@whu.edu.cn))

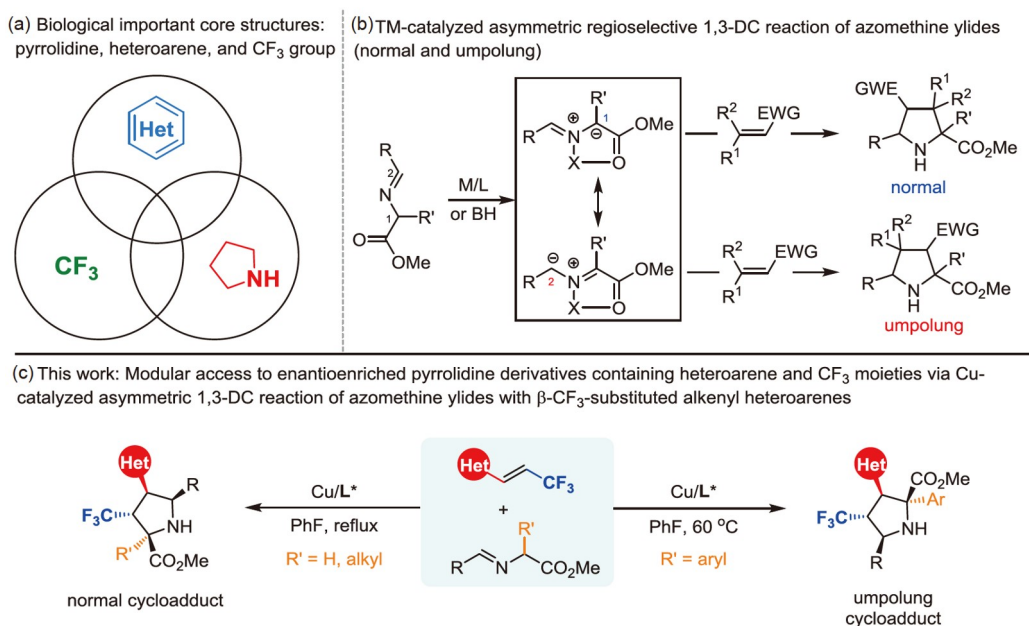
necessary and in high demand to develop efficient synthetic tactics to access chiral pyrrolidines containing both heteroarenes and trifluoromethyl groups. It would provide more opportunities for the discovery of new promising agrochemical and pharmaceutical targets to a great extent (Scheme 1a). However, successful examples involving the related facile synthetic methods have been underdeveloped until now.

On the other hand, azomethine ylides-involved transition metal-catalyzed asymmetric 1,3-dipolar cycloadditions with various strong electron-deficient alkenes have been regarded as one of the most powerful strategies for the stereo-controlled construction of chiral pyrrolidines [33–39]. To address the above unsolved synthetic problem for the preparation of high-value chiral pyrrolidines incorporating heteroarene/trifluoromethyl groups with multiple stereogenic centers, we envisioned that the  $\beta$ -CF<sub>3</sub>-substituted alkenyl heteroarenes, a type of unsymmetrically 1,2-disubstituted alkenes, could be utilized into enantioselective 1,3-dipolar cycloaddition of azomethine ylides to furnish a wide range of these important pyrrolidines. In view of their diversified reactivities, there are four challenging problems needing to be addressed in this asymmetric catalytic transformation: (1) The dipolarophiles of the 1,3-dipolar cycloaddition of azomethine ylides are mainly relied on highly-activated alkenes containing strong electron-withdrawing substituted groups. The utilization of less reactive  $\beta$ -CF<sub>3</sub>-substituted alkenyl heteroarenes may result in poor reactivity. (2) The regioselectivity control of this 1,3-dipolar cycloaddition. (3) The potential  $\beta$ -F-elimination of the trifluoromethyl group in the reaction system. (4) How to

achieve the regio- and stereoselective diversity, which is an important objective of chemical synthesis to support the research on structure-activity relationship in the fields of pharmaceuticals, agrochemicals and functional materials. The switch of the nucleophilic position of metallated-azomethine ylides at C1 or C2 would be very useful in asymmetric 1,3-dipolar cycloaddition, but only scarce examples have fulfilled this regioselectivity-control reaction (Scheme 1b) [40–47]. Xiao and Singh's group [44,47] recently discovered a substrate-controlled regiodivergent 1,3-dipolar cycloaddition of nitroolefins, in which the nucleophilic position of aldimine esters changed from C1 to C2 position when  $\alpha$ -aryl substituted aldimine esters were employed as the dipole precursors. Alternatively, regioselective control in transition metal-catalyzed asymmetric 1,3-dipolar cycloaddition of azomethine ylides could be enabled by switching different chiral ligands [45,46]. In this study,  $\beta$ -CF<sub>3</sub>-substituted alkenyl heteroarenes, a type of unsymmetrically 1,2-disubstituted alkenes bearing two different electron-deficient groups, was employed as the dipolarophiles for the first time, which should cause the challenging regioselective issue [48–51], and we serendipitously disclosed that higher temperature could afford better enantioselectivity without erosion of the diastereoselectivity. Meanwhile, a regioselective-controlled 1,3-dipolar cycloaddition was also achieved in this catalytic system (Scheme 1c).

## 2 Experimental

### General procedure for Cu-catalyzed asymmetric 1,3-dipolar



**Scheme 1** Modular access to biologically active enantioenriched pyrrolidine derivatives containing heteroarene and CF<sub>3</sub> moieties via Cu-catalyzed asymmetric 1,3-DC reaction of azomethine ylides with  $\beta$ -CF<sub>3</sub>-substituted alkenyl heteroarenes (color online).

cycloaddition of imino esters with  $\beta$ -substituted alkenyl heteroarenes. A flame dried seal tube was cooled to rt and evacuated and backfilled with nitrogen three times. Under nitrogen atmosphere, **L5** (3.9 mg, 0.005 mmol) and  $\text{Cu}(\text{OAc})_2$  (0.9 mg, 0.005 mmol) were dissolved in 1.0 mL PhF, which were stirred at appropriate temperature ( $R' = \text{H}$ , reflux;  $R' \neq \text{H}$ , 60 °C) for about 30 min. Then the imino ester **2/4** (0.15 mmol) and  $\text{Et}_3\text{N}$  (0.02 mmol) were added sequentially. Then,  $\beta$ -substituted alkenyl heteroarenes **1** (0.1 mmol) was added. When the reaction was completed (monitored by thin layer chromatography (TLC)), the organic solvent was removed and the residue was purified by column chromatography to give the desired cycloadducts, which were then directly analyzed by chiral high performance liquid chromatography (HPLC) to determine the enantiomeric excess.

### 3 Results and discussion

#### 3.1 Condition optimization

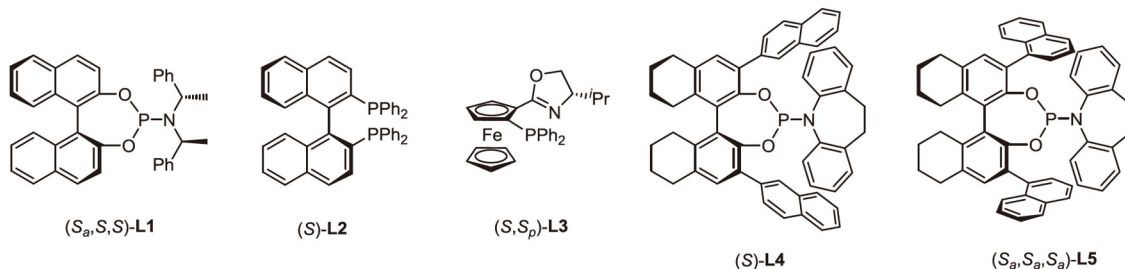
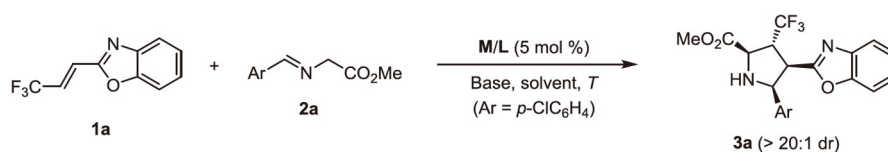
Initially, the aldimine ester **2a** and  $\beta$ - $\text{CF}_3$ -substituted alkenyl heteroarene **1a** were selected as the model substrates to investigate this catalytic asymmetric 1,3-dipolar cycloaddition using  $\text{Et}_3\text{N}$  as the base. Under the guidance of dual activated model [52], the readily available chiral phosphoramidite ligand ( $S_a, S_a, S$ )-**L1** was firstly examined and the desired normal product **3a** was obtained with perfect regioselectivity and diastereoselectivity albeit with moderate enantioselectivity (Table 1, entry 1). To further improve the level of the enantioselectivity, other kinds of chiral ligands which are often used in the asymmetric 1,3-dipolar cycloaddition were then screened (Table 1, entries 2–5). Ligand ( $S_a, S_a, S_a$ )-**L5** was proven to be optimal and gave rise to the cycloadduct **3a** in 95% yield and 70% ee at the room temperature. Since decreasing the reaction temperature was viewed as the direct and easy way to improve the enantiomeric excess in asymmetric catalysis, this Cu-catalyzed asymmetric 1,3-dipolar cycloaddition was performed at lower temperature condition. However, to our surprise, the enantioselectivity of the product **3a** was reduced to 58% at 10 °C (Table 1, entry 6). This unusual phenomenon instigated us to increase the reaction temperature. Gratifyingly, it was found that the higher temperature led to the better enantioselectivity, and up to 87% ee was obtained when the reaction was carried out at 100 °C (Table 1, entries 7–10). In addition, we also investigated the impact of metal salts and solvents (Table 1, entries 11–17), and found that  $\text{Cu}(\text{OAc})_2$  and fluorobenzene could further improve the enantioselectivity from 87% ee to 92% ee, which was determined as the optimal reaction condition (Table 1, entry 15). Finally, control experiments revealed that the cycloaddition still proceeded smoothly in the absence of the chiral ligand or the metal-complex catalyst (Table 1, entries 18–19), which demonstrates the background reaction

can be efficiently suppressed by chiral  $\text{Cu}/(S_a, S_a, S_a)$ -**L5** catalyst system even at high temperature and displayed excellent catalytic efficiency with high reactivity and stereoselective control.

#### 3.2 Substrate scope study

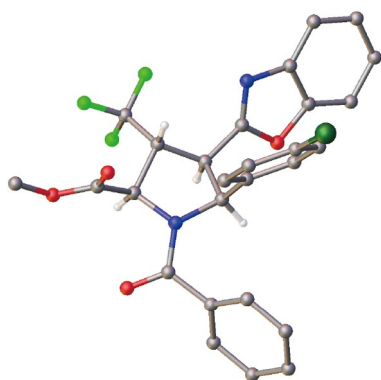
With the optimal reaction condition in hand, we explored the substrates scope of this 1,3-dipolar cycloaddition by treating (*E*)-2-(3,3,3-trifluoroprop-1-en-1-yl)benzo[*d*]oxazole **1a** with a variety of aldimine esters **2**. As shown in Table 2, when a series of electron-withdrawing groups were introduced in different positions of the aryl ring of aldimine esters, the catalytic asymmetric cycloaddition could undergo smoothly to deliver the desired cycloadducts **3a–3f** in good to high yields (89%–98%) with excellent enantioselectivities (89%–95% ee) and diastereoselectivity (>20:1 dr) (Table 2, entries 1–6). Switching the electron-withdrawing groups to electron-donating methyl or methoxyl group, the enantioselectivity of the cycloadducts **3g–3j** had a slight decline, probably due to the disfavored background reaction (Table 2, entries 7–10). The benzaldehyde-derived aldimine ester **2k** could work as a good reaction partner to give the corresponding product **3k** in high yield with good enantioselectivity (98% yield, 89% ee, Table 2, entry 11). Notably, the aldimine esters containing 1-naphthyl group (**2l**) or 2-furyl group (**2m**) were also feasible, leading to the expected products (**3l–3m**) in good reaction results (Table 2, entries 12–13). In addition, the generality of  $\beta$ - $\text{CF}_3$ -substituted alkenyl heteroarenes was then investigated (such as benzothiazole (**1b**) and 1,3-benzoxazole (**1c**) ring), and was well tolerated in the current catalytic system. The desired cycloaddition products (**3n–3o**) could be obtained in moderate to excellent results (95% yield, 90% ee; 79% yield, 87% ee, respectively, Table 2, entries 14–15). The absolute configuration of *N*-benzoylated **3a** was unambiguously determined as (2*R*,3*R*,4*R*,5*S*) by the X-ray diffraction analysis (CCDC 2266092, Figure 1).

Encouraged by the good performance of the glycine-derived aldimine esters at high temperature, we wondered whether this protocol is compatible with the less reactive  $\alpha$ -substituted aldimine esters, which is a drawback in our previous work [52]. The experimental results are summarized in the Table 3. As expected, high temperature not only enhanced the reactivity, but also induced excellent enantioselectivity for most of the  $\alpha$ -substituted aldimine esters with different alkyl substituents, including methyl (**4a**), *n*-propyl (**4b**), *i*-butyl (**4c**), benzyl (**4d**), homobenzyl (**4e**), and allyl (**4f**). The expected products **5a–5f** were successfully achieved in moderate to high yields (77%–97%) with good to excellent enantioselectivities (86%–95%) and diastereoselectivity (>20:1 dr; Table 3, entries 1–6). Other functionalized groups such as ether, thioether, ester groups (**4g–4j**)

**Table 1** Optimization of reaction conditions<sup>a)</sup>

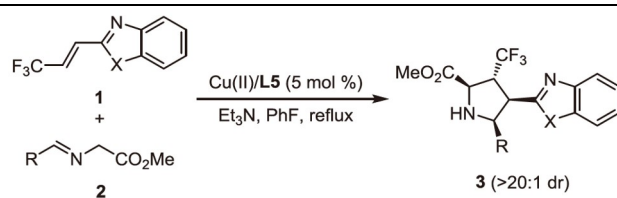
entry	[M]	L*	solvent	base	T (°C)	yield (%) <sup>b)</sup>	ee (%) <sup>c)</sup>
1	CuBF <sub>4</sub>	(S <sub>a</sub> ,S,S)-L1	Toluene	Et <sub>3</sub> N	25	26	64
2	CuBF <sub>4</sub>	(S)-L2	Toluene	Et <sub>3</sub> N	25	5	20
3	CuBF <sub>4</sub>	(S,S <sub>p</sub> )-L3	Toluene	Et <sub>3</sub> N	25	98	44
4	CuBF <sub>4</sub>	(S)-L4	Toluene	Et <sub>3</sub> N	25	93	63
5	CuBF <sub>4</sub>	(S <sub>a</sub> ,S <sub>a</sub> ,S <sub>a</sub> )-L5	Toluene	Et <sub>3</sub> N	25	95	70
6	CuBF <sub>4</sub>	(S <sub>a</sub> ,S <sub>a</sub> ,S <sub>a</sub> )-L5	Toluene	Et <sub>3</sub> N	10	96	58
7	CuBF <sub>4</sub>	(S <sub>a</sub> ,S <sub>a</sub> ,S <sub>a</sub> )-L5	Toluene	Et <sub>3</sub> N	50	95	77
8	CuBF <sub>4</sub>	(S <sub>a</sub> ,S <sub>a</sub> ,S <sub>a</sub> )-L5	Toluene	Et <sub>3</sub> N	90	93	84
9	CuBF <sub>4</sub>	(S <sub>a</sub> ,S <sub>a</sub> ,S <sub>a</sub> )-L5	Toluene	Et <sub>3</sub> N	100	95	87
10	CuBF <sub>4</sub>	(S <sub>a</sub> ,S <sub>a</sub> ,S <sub>a</sub> )-L5	Toluene	Et <sub>3</sub> N	120	87	83
11	CuPF <sub>6</sub>	(S <sub>a</sub> ,S <sub>a</sub> ,S <sub>a</sub> )-L5	Toluene	Et <sub>3</sub> N	100	97	77
12	CuOAc	(S <sub>a</sub> ,S <sub>a</sub> ,S <sub>a</sub> )-L5	Toluene	Et <sub>3</sub> N	100	98	89
13	AgOAc	(S <sub>a</sub> ,S <sub>a</sub> ,S <sub>a</sub> )-L5	Toluene	Et <sub>3</sub> N	100	98	53
14	Cu(OAc) <sub>2</sub>	(S <sub>a</sub> ,S <sub>a</sub> ,S <sub>a</sub> )-L5	Toluene	Et <sub>3</sub> N	100	98	89
15	Cu(OAc) <sub>2</sub>	(S <sub>a</sub> ,S <sub>a</sub> ,S <sub>a</sub> )-L5	Fluorobenzene	Et <sub>3</sub> N	reflux	98	92
16	Cu(OAc) <sub>2</sub>	(S <sub>a</sub> ,S <sub>a</sub> ,S <sub>a</sub> )-L5	1,4-Dioxane	Et <sub>3</sub> N	reflux	93	4
17	Cu(OAc) <sub>2</sub>	(S <sub>a</sub> ,S <sub>a</sub> ,S <sub>a</sub> )-L5	1,2-dichloroethane	Et <sub>3</sub> N	reflux	88	89
18	Cu(OAc) <sub>2</sub>	–	Fluorobenzene	Et <sub>3</sub> N	reflux	90	–
19	–	–	Fluorobenzene	Et <sub>3</sub> N	reflux	62	–

a) All reactions were carried out with 0.10 mmol of **1a**, 0.15 mmol of **2a**, 0.005 mmol of **M/L** and 0.02 mmol of the base in 1 mL of solvent for 8–12 h. CuBF<sub>4</sub> = Cu(MeCN)<sub>4</sub>BF<sub>4</sub>. dr was determined by crude <sup>1</sup>H NMR. b) Isolated yield. c) ee was determined by HPLC analysis.

**Figure 1** X-ray structure of benzoylated (2R,3R,4R,5S)-**3a** (color online).

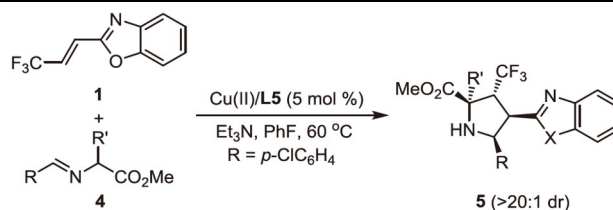
could be well tolerated under this condition, leading to the corresponding  $\alpha$ -substituted cycloadducts (**5g–5j**) in 80%–98% yields with 84%–95% ee. The cyclic aldimino ester **4k** derived from ( $\pm$ )-homoserine was also compatible, affording the target compound **5k** containing a unique spiro N-quaternary stereocenter in 98% yield with 91% ee. Notably, the challenging alkyl substrate cyclohexanecarboxaldehyde derived  $\alpha$ -methyl aldimine ester (**4l**) was also feasible. The expected product **5l** could be formed in 97% yield with 88% ee (Table 3, entry 12).

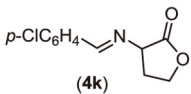
On the basis of these promising results, we next turn our attention to  $\alpha$ -aryl substituted aldimine esters as the precursors of azomethine ylides. As shown in Scheme 2, three

**Table 2** Substrate scope of imino esters and  $\beta$ -substituted alkenyl heteroarenes<sup>a)</sup>

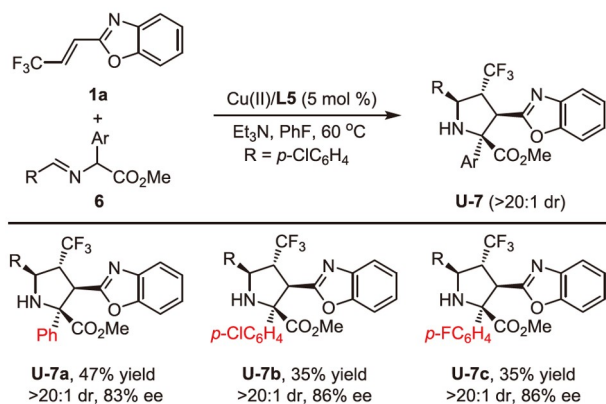
entry	R	X	<b>3</b>	yield (%) <sup>b)</sup>	ee (%) <sup>c)</sup>
1	<i>p</i> -ClC <sub>6</sub> H <sub>4</sub> ( <b>2a</b> )	O ( <b>1a</b> )	<b>3a</b>	98	92
2	<i>o</i> -ClC <sub>6</sub> H <sub>4</sub> ( <b>2b</b> )	O ( <b>1a</b> )	<b>3b</b>	89	89
3	<i>m</i> -ClC <sub>6</sub> H <sub>4</sub> ( <b>2c</b> )	O ( <b>1a</b> )	<b>3c</b>	93	89
4	<i>p</i> -BrC <sub>6</sub> H <sub>4</sub> ( <b>2d</b> )	O ( <b>1a</b> )	<b>3d</b>	90	89
5	<i>p</i> -CNC <sub>6</sub> H <sub>4</sub> ( <b>2e</b> )	O ( <b>1a</b> )	<b>3e</b>	97	95
6	<i>p</i> -NO <sub>2</sub> C <sub>6</sub> H <sub>4</sub> ( <b>2f</b> )	O ( <b>1a</b> )	<b>3f</b>	96	92
7	<i>p</i> -MeC <sub>6</sub> H <sub>4</sub> ( <b>2g</b> )	O ( <b>1a</b> )	<b>3g</b>	95	80
8	<i>o</i> -MeC <sub>6</sub> H <sub>4</sub> ( <b>2h</b> )	O ( <b>1a</b> )	<b>3h</b>	94	79
9	<i>m</i> -MeC <sub>6</sub> H <sub>4</sub> ( <b>2i</b> )	O ( <b>1a</b> )	<b>3i</b>	86	73
10	<i>p</i> -MeOC <sub>6</sub> H <sub>4</sub> ( <b>2j</b> )	O ( <b>1a</b> )	<b>3j</b>	87	75
11	Ph ( <b>2k</b> )	O ( <b>1a</b> )	<b>3k</b>	98	89
12	1-naphthyl ( <b>2l</b> )	O ( <b>1a</b> )	<b>3l</b>	95	80
13	2-furyl ( <b>2m</b> )	O ( <b>1a</b> )	<b>3m</b>	72	89
14	<i>p</i> -ClC <sub>6</sub> H <sub>4</sub> ( <b>2a</b> )	S ( <b>1b</b> )	<b>3n</b>	95	90
15	<i>p</i> -ClC <sub>6</sub> H <sub>4</sub> ( <b>2a</b> )	NMe ( <b>1c</b> )	<b>3o</b>	79	87

a) All reactions were carried out with 0.10 mmol of **1**, 0.15 mmol of **2**, 0.005 mmol of Cu/L5 and 0.02 mmol of the Et<sub>3</sub>N in 1 mL of PhF at 100 °C for 8–12 h. Cu(II) = Cu(OAc)<sub>2</sub>. dr was determined by crude <sup>1</sup>H NMR. b) Isolated yield. c) ee was determined by HPLC analysis.

**Table 3** Substrate scope of  $\alpha$ -alkyl-substituted imino esters<sup>a)</sup>

entry	R	R'	<b>5</b>	yield (%) <sup>b)</sup>	ee (%) <sup>c)</sup>
1	<i>p</i> -ClC <sub>6</sub> H <sub>4</sub>	Me ( <b>4a</b> )	<b>5a</b>	95	95
2	<i>p</i> -ClC <sub>6</sub> H <sub>4</sub>	<i>n</i> -Pr ( <b>4b</b> )	<b>5b</b>	89	92
3	<i>p</i> -ClC <sub>6</sub> H <sub>4</sub>	<i>i</i> -Bu ( <b>4c</b> )	<b>5c</b>	77	91
4	<i>p</i> -ClC <sub>6</sub> H <sub>4</sub>	PhCH <sub>2</sub> ( <b>4d</b> )	<b>5d</b>	97	94
5	<i>p</i> -ClC <sub>6</sub> H <sub>4</sub>	PhCH <sub>2</sub> CH <sub>2</sub> ( <b>4e</b> )	<b>5e</b>	87	86
6	<i>p</i> -ClC <sub>6</sub> H <sub>4</sub>	allyl ( <b>4f</b> )	<b>5f</b>	96	86
7	<i>p</i> -ClC <sub>6</sub> H <sub>4</sub>	<i>t</i> BuOCH <sub>2</sub> ( <b>4g</b> )	<b>5g</b>	98	84
8	<i>p</i> -ClC <sub>6</sub> H <sub>4</sub>	MeSCH <sub>2</sub> CH <sub>2</sub> ( <b>4h</b> )	<b>5h</b>	80	93
9	<i>p</i> -ClC <sub>6</sub> H <sub>4</sub>	MeO <sub>2</sub> CCH <sub>2</sub> ( <b>4i</b> )	<b>5i</b>	99	92
10	<i>p</i> -ClC <sub>6</sub> H <sub>4</sub>	MeO <sub>2</sub> C(CH <sub>2</sub> ) <sub>2</sub> ( <b>4j</b> )	<b>5j</b>	86	95
11 <sup>d)</sup>	<i>p</i> -ClC <sub>6</sub> H <sub>4</sub>		<b>5k</b>	98	91
12 <sup>e)</sup>	Cy	Me ( <b>4l</b> )	<b>5l</b>	97	88

a) All reactions were carried out with 0.1 mmol of **1**, 0.15 mmol of **4**, 0.005 mmol of Cu/(S<sub>a</sub>,S<sub>a</sub>,S<sub>a</sub>)-L5 and 0.02 mmol of Et<sub>3</sub>N in 1 mL of PhF for 8–12 h. b) Yields refer to the isolated products after chromatographic purification. c) The dr value was determined by crude <sup>1</sup>H NMR, and the ee value was determined by HPLC analysis. d) *t*BuOK was used instead of Et<sub>3</sub>N. e) R = Cyclohexyl.



**Scheme 2** Substrate scope of  $\alpha$ -aryl-substituted imino esters (color online).

$\alpha$ -aryl substituted aldimine esters **6a–6c** were employed as the dipole precursors under the standard reaction condition. To our delight, the umpolung cycloadducts **U-(7a–7c)** could be obtained smoothly in moderate yield with good enantioselectivity and excellent regioselectivity and diastereoselectivity (35%–47% yields, 83%–86% ee, >20:1 dr, >20:1 rr). The delocalization of negative charge would migrate from the C1 position of the azomethine ylides to C2 position, and thus furnishing umpolung reactivity and regioselectivity with the enhanced steric hindrance at C1-position (*vide infra*). The relative configuration of the racemic **U-7a** was determined by the X-ray diffraction analysis, which could further verify the umpolung reactivity at high reaction temperature (CCDC 2266096, [Figure 2](#)).

### 3.3 A computational study on the reaction mechanism catalyzed by the Cu(I) species

To shed more mechanistic insight on the Cu-catalyzed enantio- and regioselective cycloaddition reaction with the substrate **2a** or **6a** to form **3a** or umpolung-type **U-7a** ([Figure 3a](#)), respectively, systematic DFT calculations (mainly M06-L method with mixed basis sets (SDD plus its effective core potentials for Cu and 6-31G\* for the other atoms)) were carried out [52–75]. We first discuss our results using the neutral Cu(I)-azomethine ylide complex Cu(I)-**L5** (containing **L5** and deprotonated **2a**) with dipolarophile **1a** as the computational model, whereas the discouraging enantio- and regioselective results were computed to be achieved by the corresponding neutral Cu(II)-**L5**-catalyzed system (*vide infra*).

As shown in our previous work [52] and [Figure 3b](#), the Cu(I)-**L5** complex has two possible three-coordinate isomers (**L5**<sub>2a1</sub> and **L5**<sub>2a2</sub>). The isomer **L5**<sub>2a1</sub> was computed to be 1.8 kcal/mol lower in free energy than **L5**<sub>2a2</sub>, due to larger steric repulsion between the extended *p*-ClC<sub>6</sub>H<sub>4</sub> and bulky amido moieties in **L5**<sub>2a2</sub>. In addition, the reacting C1 atom in **L5**<sub>2a1</sub>

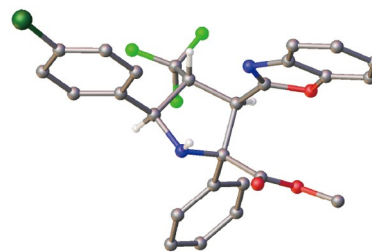


**Figure 2** X-ray structure of *rac*-**U-7a** (relative configuration) (color online).

and **L5**<sub>2a2</sub> has a more negative charge (−0.22) than the other reacting C2 atom (0.01), which suggests a higher nucleophilic character for C1 atom than C2 atom ([Scheme 1b](#)).

Our DFT results further show that this Cu(I)-**L5** catalyzed model follows the two-step mechanism. For the normal regioselective cycloaddition pathway forming the cycloadducts **3a** and **3aent** ([Figure 4a](#)), the dipolarophile N atom was first coordinated to the Cu(I) center to form four-coordinate intermediates **IN1**<sub>3a</sub> and **IN1**<sub>3aent</sub>. The rigid and bulky phosphoramidite ligand offers a chiral pocket around the metal center along with one vacant zone for the coordination and stacking of the two substrates ([Figure 3d](#)). Then, the C1–C3 bond was initially formed to give zwitterionic intermediates **IN2**<sub>3a</sub> and **IN2**<sub>3aent</sub> via Michael-addition transition states **TS1**<sub>3a</sub> and **TS1**<sub>3aent</sub>, respectively. Afterward, the second C2–C4 bond completed and formed the cycloaddition product via the rate-determining cyclization transition states **TS2**<sub>3a</sub> and **TS2**<sub>3aent</sub>. The overall barrier for this process forming the major product **3a** is lower than its enantiomeric product **3aent** by approximately 3.1 kcal/mol (by the SMD M06-L//M06-L method), which is qualitatively consistent with the experiment.

As depicted in [Figure 4b](#), **1a** attacks from the upper side of the azomethine ylide in **TS2**<sub>3a</sub> leading to the major product **3a**. However, the formation of the minor product **3aent** requires the downward attack of the ylide in **TS2**<sub>3aent</sub>, which experiences more steric repulsion between the larger benzo [*d*]oxazole and H<sub>4</sub>-naphthol groups. This is also verified by a much larger change of a key dihedral angle 1 (−66° in **TS2**<sub>3aent</sub> vs. −125° in **L5**<sub>2a1</sub>). Finally, ligand exchange of the product **3a** or **3aent** by another azomethine molecule (**2a**) completes the catalytic cycle and regenerates the active species **L5**<sub>2a1</sub>. The overall reaction was found to be exergonic by about 0.1 kcal/mol.

Whereas, for the formation of the reversal regioselective (umpolung-type) product **U-3a**, the initial C2–C3 bond-forming step via **U-TS1**<sub>3a2</sub> was computed to be the rate-determining step with the barrier of about 17.1 kcal/mol, which is higher than the favorable major pathway via **TS2**<sub>3a</sub> by 5.6 kcal/mol ([Figure 4a](#)), mainly due to the formation of less stable zwitterionic intermediate **U-IN2**<sub>3a2</sub> ( $\Delta G_{\text{soln}} = 10.6$  kcal/mol vs. 5.0 kcal/mol for **IN2**<sub>3a</sub>). A lower thermostability

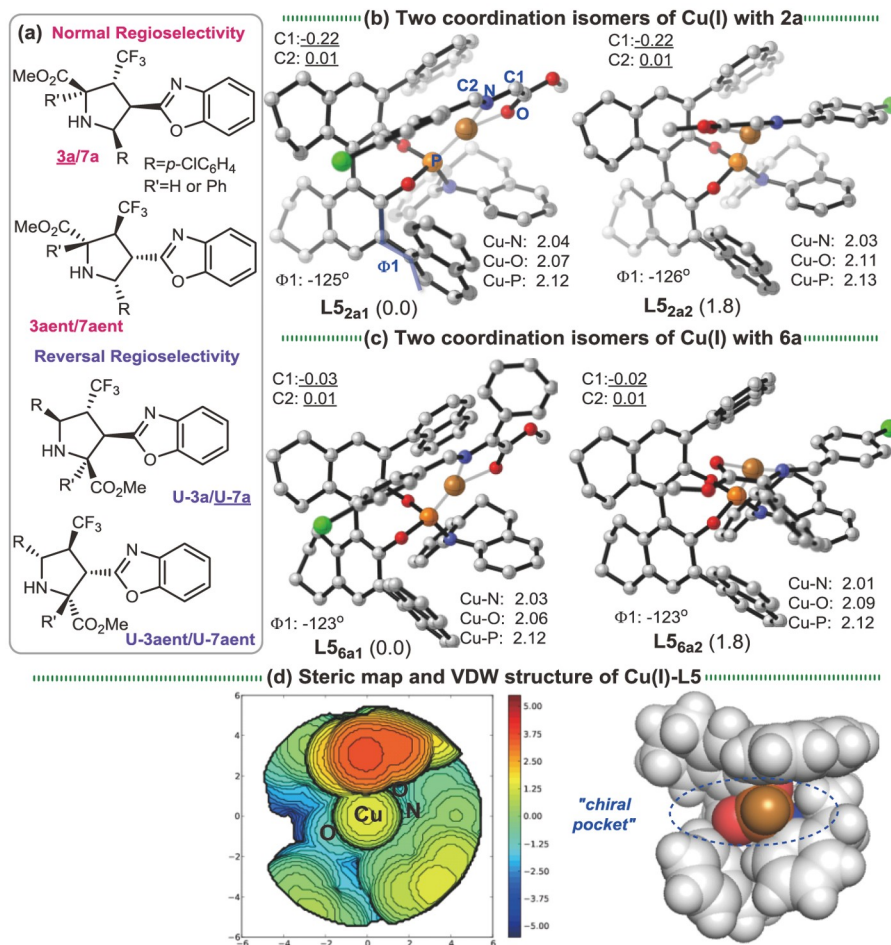


**Figure 3** Structural models. (a) Different possible products for the Cu-catalyzed dipolar cycloaddition with the substrate **2a** or **6a**. (b) Two possible coordination isomers in the Cu(I)-azomethine ylide complex (**L5<sub>2a1</sub>** and **L5<sub>2a2</sub>**; **L5<sub>6a1</sub>** and **L5<sub>6a2</sub>**). The relative free energies (in kcal/mol) in fluorobenzene solution by the SMD M06-L//M06-L method, key bond lengths (in Å) and NPA charge (underlined) of the two reacting carbon (C1 and C2) atoms in gas phase are given. (c) Steric map (left; red (more bulky) and blue (less bulky)) and VDW structure of the optimized intermediate **L5<sub>2a1</sub>** with omission of the substrate (color online).

in **U-IN2<sub>3a</sub>** should partly attribute to the missing  $\pi$ - $\pi$  stacking between the heteroarene rings of the two substrates. Therefore, the thermostability of the zwitterionic intermediates **IN2** derived from the first-addition step plays a vital role in the regioselectivity.

Interestingly, when the H atom on the C1 atom of the dipole substrate was replaced by one Ph group in substrate **6a**, our DFT results reveal that both electronic and steric effects by the new Ph group alter the reaction energetics and outcomes. Notably, the computed atomic NPA charge on the reacting C1 atom in **L5<sub>6a1</sub>** and **L5<sub>6a2</sub>** becomes much less negative (−0.02—0.03 vs. −0.22 in **L5<sub>2a1</sub>** and **L5<sub>2a2</sub>**, Figure 3b, c), due to additional delocalization to the Ph group. Whereas, the computed atomic NPA charge on the other reacting C2 atom is the same (0.01) in **L5<sub>2a1</sub>**, **L5<sub>2a2</sub>**, **L5<sub>6a1</sub>** and **L5<sub>6a2</sub>**. As a result, the computed atomic NPA charges between the C1 and C2 atoms (involving the first addition step in the normal and reversal regioselective pathways, respectively) become very small in **L5<sub>6a1</sub>** and **L5<sub>6a2</sub>**. These results

suggest that the introduction of the new Ph group on C1 should significantly reduce nucleophile character for the C1 atom of the dipole part and render similar reactivity/nucleophilic character for both the reacting C1 and C2 atoms responsible for the two different regioselective pathways.

Our results also support that the reaction preferentially gives the reversal regioselective cycloaddition product **U-7a**. This umpolung-type pathway has a lower reaction barrier than the normal pathway to form **7a** by 7.1 kcal/mol (Figure 5a, b). The final cyclization step in the normal and reversal pathways via **TS2<sub>7a</sub>** and **U-TS2<sub>7a2</sub>**, respectively, become the rate-determining step. Moreover, the reaction barrier via **U-TS2<sub>7aent</sub>** forming **U-7aent** (the enantiomeric product of **U-7a**) is about 21.6 kcal/mol, higher than **U-TS2<sub>7a2</sub>** by 5.7 kcal/mol, due to the increased steric repulsion between the larger benzo[*d*]oxazole and H<sub>4</sub>-naphthol groups.

In comparison with the reaction of **2a**, several key energetic changes for the reaction of **6a** were also noticed. (1) The first-step barrier for the normal pathway via **TS1** is

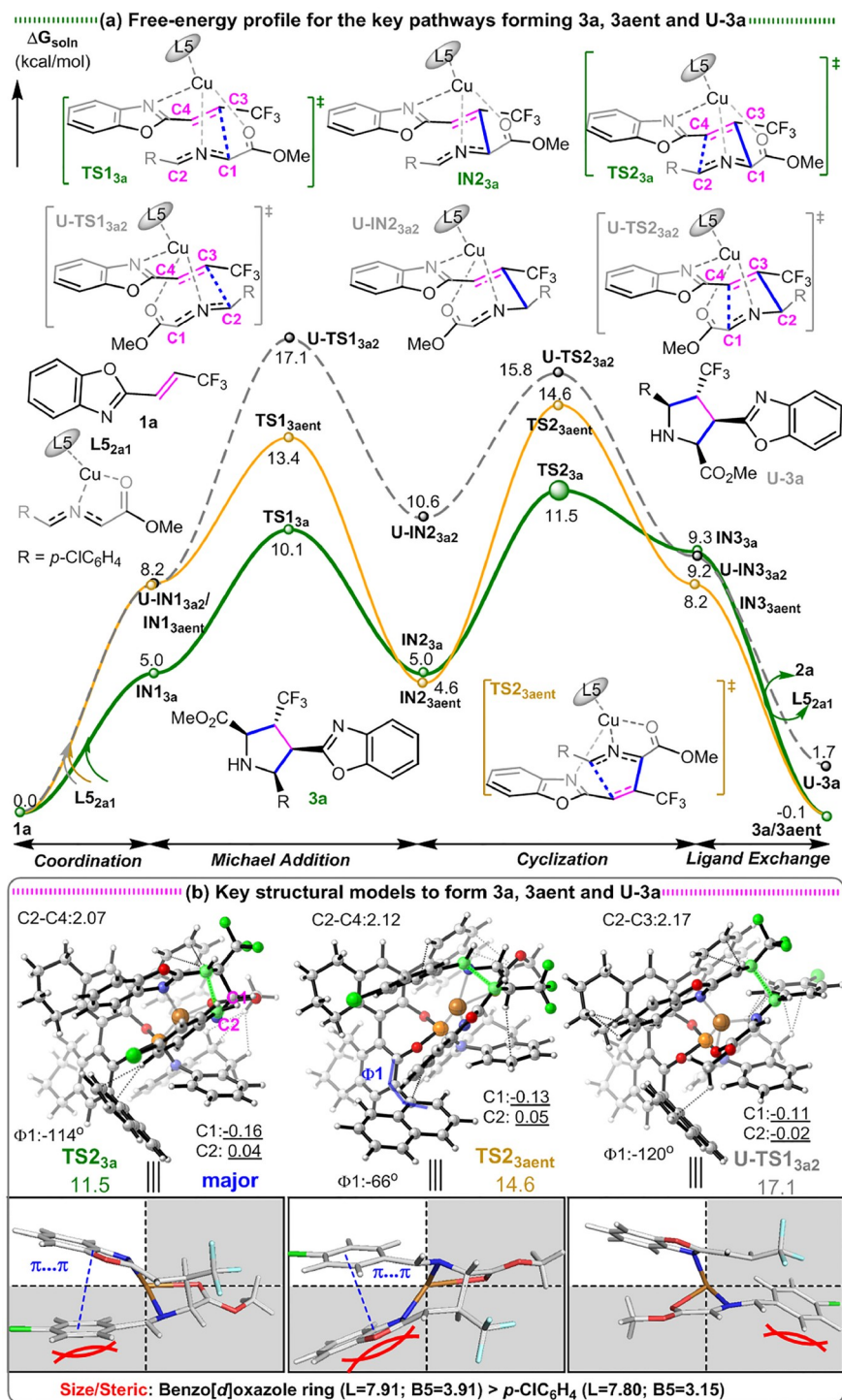


**Figure 4** Key reaction pathways and stereo-induction models. (a) Free-energy profile for the key pathways to form 3a, 3aent and U-3a in solution by the SMD M06-L//M06-L method. (b) key structural models with key bond lengths (in Å), NPA charge (underlined) of the two carbon atoms, key dihedrals, steric parameters (L and B5 by sterimol) of the heteroarene rings and relative free energies (in kcal/mol) in the solution by the SMD M06-L//M06-L method are also given (color online).

raised (10.1→16.5 kcal/mol), while that for the reversed pathway is slightly decreased (17.1→15.9 kcal/mol). (2) The first-addition intermediate **IN2** also becomes unstable (5.0→14.6 kcal/mol) for the normal pathway, but becomes more stable for the reversed pathway (10.6→8.9 kcal/mol).

Consequently, the normal first-addition intermediate **IN2**<sub>7a</sub> becomes less stable than the abnormal intermediate **U-IN2**<sub>7a2</sub> by 5.7 kcal/mol. (3) The second-step barrier for the reversed pathway (via **U-TS2**) is only slightly increased (15.8→15.9 kcal/mol), while that for the normal pathway (via **TS2**) is



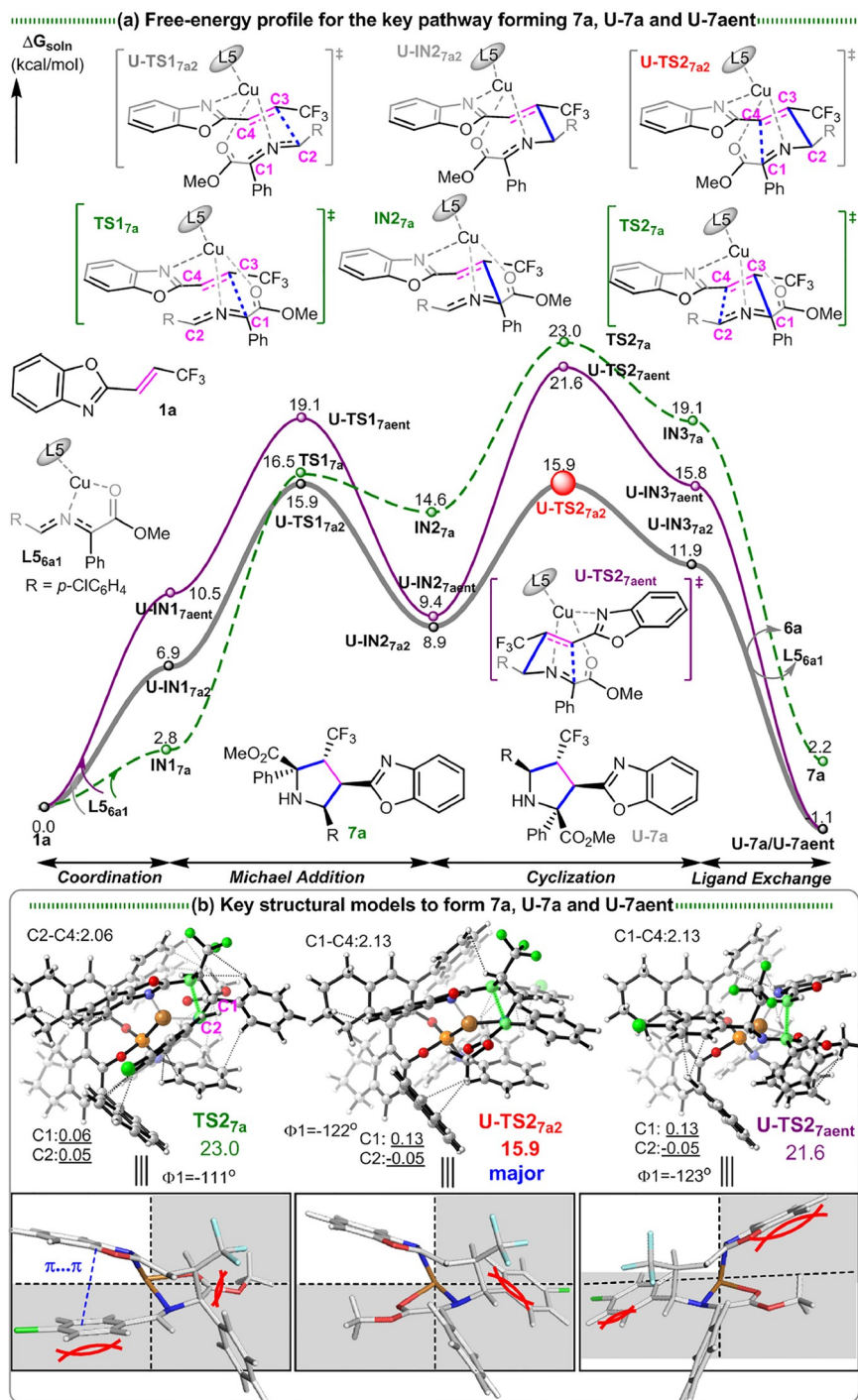


**Figure 5** Key pathways and stereo-induction models. (a) Free-energy profile for the key pathways to form **7a**, **U-7a** and **U-7aent** in the solution by the SMD M06-L//M06-L method. (b) Key structural models with key bond lengths (in Å), NPA charge (underlined) of the two carbon atoms and relative free energies (in kcal/mol) in the solution by the SMD M06-L//M06-L method are also given (color online).

considerably increased (11.5→23.0 kcal/mol). (4) The cyclization intermediate **IN3** for the reversal pathway becomes less unstable (9.2→11.9 kcal/mol), while it becomes much more unstable for the normal pathway (9.3→19.1 kcal/mol). In addition, the thermostability of the cycloadducts (**3a**→**7a**) for the normal pathway becomes less favorable (−0.1→2.2

kcal/mol), but those for the reverse pathway (*i.e.*, **U-3a**→**U-7a**) becomes slightly more favorable (1.7→−1.1 kcal/mol). The normal pathway obviously destabilized by the introduction of the Ph group should be resulted from the lower nucleophilic character for the C1 atom (*vide supra*) as well as more steric repulsion (*vide infra*). Again, the thermostability

of the zwitterionic intermediates **IN2** derived from the first C–C forming step or the cycloadducts (**3** or **7**) is the key factor in determining the regioselectivity.

### 3.4 Analysis of the enantioselectivity and regioselectivity

To further understand the origin of these enantio- and regioselectivity, relative distortion/interaction analysis [70,76–79] of the critical enantio- and regio-determining transition states was performed (Figure 6). Our results indicated that **TS2**<sub>3aent</sub> (forming the minor product **3aent**) has a slightly larger interaction energy than **TS2**<sub>3a</sub> (giving the major product **3a** ( $\Delta\Delta G_{\text{int}}^{\ddagger} = 0.5$  kcal/mol)), but its higher distortion energy in **TS2**<sub>3aent</sub> ( $\Delta\Delta G_{\text{dist}}^{\ddagger} = 2.7$  kcal/mol) is the crucial factor in dictating the enantioselectivity. As shown in Figure 4b, the higher distortion energy should relate to the more steric repulsion between the large benzo[*d*]oxazole and H<sub>4</sub>-naphthol parts (the dihedral angle 1: from  $-125^{\circ}$  in **L5**<sub>2a1</sub> to  $-66^{\circ}$  in **TS2**<sub>3aent</sub> ( $-114^{\circ}$  in **TS2**<sub>3a</sub>)). These results showed that the steric effect plays a key role in controlling the enantioselectivity for the formation of **3a**. Additionally, although lower distortion energy was found in the reversal pathway via **U-TS1**<sub>3a2</sub> ( $\Delta\Delta G_{\text{dist}}^{\ddagger} = 1.4$  kcal/mol), its smaller interaction energy than the major pathway via **TS1**<sub>3a</sub> by 7.5 kcal/mol is the major factor to disfavor the reversal pathway. The diminished interaction energy in **U-TS1**<sub>3a2</sub> can partially attribute to the absence/missing of  $\pi$ - $\pi$  stacking between the benzo[*d*]oxazole and *p*-ClC<sub>6</sub>H<sub>4</sub> rings on the two substrates in the reversal pathway.

For the reaction with **6a**, even though **TS2**<sub>7a</sub> has a higher interaction energy than **U-TS2**<sub>7a2</sub> ( $\Delta\Delta G_{\text{int}}^{\ddagger} = 7.1$  kcal/mol), its distortion energy is also higher than **U-TS2**<sub>7a2</sub> ( $\Delta\Delta G_{\text{dist}}^{\ddagger} = 7.3$  kcal/mol) and **TS2**<sub>3a</sub> (by 9.7 kcal/mol). Such increasing distortion energy in **TS2**<sub>7a</sub> should be resulted from more repulsion between the new Ph and tertiary CF<sub>3</sub> groups as well

as the Ph ring and amido group on **L5**<sub>6a1</sub> (Figure 5b). Overall, our results also showed that both steric and electronic effects control the enantio- and regioselectivity for this 1,3-dipolar addition. The introduction of the Ph group on the C1 atom of the dipole not only decreases its nucleophilic character for the normal regioselective pathway, but also creates severe steric congestion between the Ph and CF<sub>3</sub> groups. Hence, the normal regioselective pathway has to overcome a higher reaction barrier and decrease the stability of the cycloadduct, which switches to undergo the reversal regioselectivity. These computational results are qualitatively consistent with the observed enantio- and regioselectivity in the experiment (entry 1 in Table 2 and Scheme 2). Notably, the other common DFT methods (PBE0-D3, B3LYP-D3, M06-D3) also supported the above-mentioned computational results.

### 3.5 Reaction mechanism catalyzed by the Cu(II) species

Extensive DFT calculations were also carried out for the mechanism catalyzed by the neutral Cu(II) species (containing **L5**, deprotonated **2a** and one CH<sub>3</sub>CO<sub>2</sub><sup>−</sup> molecular) [64,80]. The Cu(II)-**L5** complex has four possible five-coordinate isomers (<sup>2</sup>**L5**<sub>2a1</sub>, <sup>2</sup>**L5**<sub>2a2</sub>, <sup>2</sup>**L5**<sub>2a3</sub> and <sup>2</sup>**L5**<sub>2a4</sub>, see Figure S7, Supporting Information online) in our calculations. As shown in Figures S8–S12 and Table S3 (Supporting Information online), we have explored different conformations or coordination modes for the cycloaddition steps. However, different DFT methods for the Cu(II) catalytic model prefer to give the minor product **3aent** over the major product **3a** (Table 4), which is inconsistent with the experimental results. Furthermore, different DFT methods also suggested that this Cu(II) reaction tends to give the product **7aent** or **7a** (Table S4), instead of the desired uncommon product **U-7a** (Scheme 2). Therefore, our calculations suggest that the mechanism catalyzed by the Cu(II)-**L5** model should be excluded in this

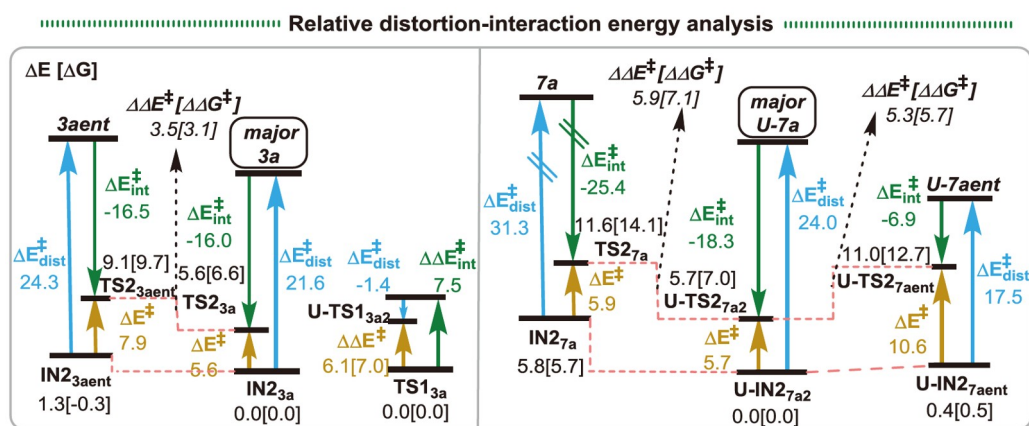


**Figure 6** Relative distortion-interaction energy analysis for the key enantio- and regio-determining transition states for the two different substrates (relative to their precursor intermediates, except for **TS1**<sub>3a</sub> and **U-TS1**<sub>3a2</sub>;  $E_{\text{dist}}^{\ddagger}$ : total distortion energy;  $E_{\text{int}}^{\ddagger}$ : interaction energy) by the SMD M06-L//M06-L method. All values are the relative electronic energy in the solution except the values in square brackets, which are the relative free energies (kcal/mol) (color online).

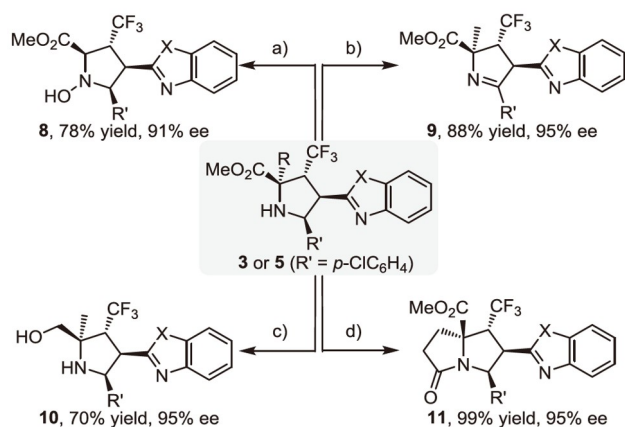
1,3-dipolar addition and the Cu(II)-L5 is possibly reduced to Cu(I)-L5 by electron-rich molecules during the reaction process [81–83]. A higher temperature might facilitate such metal reduction and selectivity, which a more in-depth mechanistic study is required.

### 3.6 Synthetic elaborations

In order to demonstrate the synthetic potential of this protocol, a series of synthetic transformations of the cycloadduct products were performed. As shown in Scheme 3, utilizing *m*-CPBA (*m*-chloroperbenzoic acid) or DDQ (2,3-dichloro-5,6-dicyano-1,4-benzoquinone) as the oxidant, *N*-hydroxyl pyrrolidine **8** and cyclic imine **9** could be respectively obtained without loss of diastereo- and enantiomeric excess. Reduction of **5a** with NaBH<sub>4</sub> would deliver the corresponding amino alcohol **10** in 70% yield with maintained enantio- and diastereoselectivity. Treating **5j** with AcOH could efficiently prepare tetrahydro-1H-pyrrolizine derivative **11** in 99% yield and without erosion of stereoselectivity.

**Table 4** The free-energy barriers (in kcal/mol) of the most favorable reaction pathway for the cycloaddition reactions catalyzed by the Cu(II) species by different SMD methods based on the M06-L-optimized structures. The results marked in red have the lowest barrier

	M06-L	PBE0-D3	B3LYP-D3	M06-D3
<b>3a</b>	23.5	16.2	19.9	11.3
<b>3aent</b>	22.3	15.3	17.6	10.3
<b>U-3a</b>	28.5	21.9	23.9	16.8
<b>U-3aent</b>	33.0	28.6	28.8	22.3
<b>7a</b>	28.8	19.0	25.3	13.1
<b>7aent</b>	30.8	17.3	21.7	10.5
<b>U-7a</b>	30.3	19.9	24.2	13.2
<b>U-7aent</b>	36.3	24.8	30.8	19.4



**Scheme 3** Synthetic elaborations. Reaction conditions: a) *m*-CPBA, DCM, rt (R = H); b) DDQ, toluene, 50 °C (R = Me); c) NaBH<sub>4</sub>, MeOH, rt (R = Me); d) AcOH; toluene, rt (R = (CH<sub>2</sub>)<sub>2</sub>CO<sub>2</sub>Me).

## 4 Conclusions

In conclusion, we have developed a temperature-dependent Cu-catalyzed enantioselective 1,3-dipolar cycloaddition of azomethine ylides with β-CF<sub>3</sub>-substituted alkenyl heteroarenes, affording a variety of chiral pyrrolidine derivatives containing both heteroarenes and trifluoromethyl group with multiple stereogenic centers in high yield with exclusive diastereoselectivity and excellent enantioselectivity. The unique phenomenon that the higher reaction temperature led to better asymmetric induction was intriguing, which efficiently extended the substrate scope to the less reactive α-substituted aldimine esters. Meanwhile, umpolung-type (3 +2)-cycloaddition could be realized with α-aryl substituted aldimine esters with the current protocol. Our systematic DFT investigation revealed that the thermostability of the cycloadducts determines the origin of stereo- and regioselectivity of this 1,3-dipolar cycloaddition, and suggested that copper(I) might be responsible for the catalytic system, although copper(II) salt was utilized.

**Acknowledgements** This work was supported by the National Natural Science Foundation of China (22071186, 22071187, 22073067, 22101216, 22271226, 21933003, 22193020, 22193023), the National Youth Talent Support Program, the Natural Science Foundation of Hubei Province (2020CFA036 2021CFA069), the Fundamental Research Funds for the Central Universities (2042022kf1180, 2042022kf1040), the Shenzhen Nobel Prize Scientists Laboratory Project (C17783101) and the Guangdong Provincial Key Laboratory of Catalytic Chemistry (2020B121201002). We thank the Center for Computational Science and Engineering at the Southern University of Science and Technology and CHEM HPC at SUSTech for partly supporting this work.

**Conflict of interest** The authors declare no conflict of interest.

**Supporting information** The supporting information is available online at [chem.scichina.com](http://chem.scichina.com) and [link.springer.com/journal/11426](http://link.springer.com/journal/11426). The supporting materials are published as submitted, without typesetting or editing. The responsibility for scientific accuracy and content remains entirely with the authors.

- Enders D, Thiebies C. *Pure Appl Chem*, 2001, 73: 573–578
- Harwood LM, Vickers RJ. in *Synthetic Applications of 1,3-Dipolar Cycloaddition Chemistry Toward Heterocycles and Natural Products*. Padwa A and Pearson W, eds. Hoboken: John Wiley & Sons, Ltd., 2002
- Pyne S, Davis A, Gates N, Hartley J, Lindsay K, Machan T, Tang M. *Synlett*, 2004, 2004: 2670–2680
- Michael JP. *Nat Prod Rep*, 2008, 25: 139–165
- Mukaiyama T, Asami M. *Top Curr Chem*, 1985, 127: 133–167
- Vicario JL, Badia D, Carrillo L, Ruiz N, Reyes E. *Targets Heterocyclic Syst*, 2008, 12: 302–327
- Bhat C, Tilve SG. *RSC Adv*, 2014, 4: 5405–5452
- Sulzer-Mossé S, Alexakis A. *Chem Commun*, 2007, 30: 3123–3135
- Jensen KL, Dickmeiss G, Jiang H, Albrecht L, Jørgensen KA. *Acc Chem Res*, 2012, 45: 248–264
- Li X, Li J. *Mini-Rev Med Chem*, 2010, 10: 794–805
- Vega-Peñalosa A, Paria S, Bonchio M, Dell'Amico L, Companyó X. *ACS Catal*, 2019, 9: 6058–6072
- Cossy J, Pardo DG. *Targets Heterocyclic Syst*, 2002, 6: 1–26

- 13 Chelucci G, Murineddu G, Pinna GA. *Tetrahedron-Asymmetry*, 2004, 15: 1373–1389
- 14 Liu X, Lin L, Feng X. *Org Chem Front*, 2014, 1: 298–302
- 15 Daly JW. *J Med Chem*, 2003, 46: 445–452
- 16 Harrity JPA, Provoost O. *Org Biomol Chem*, 2005, 3: 1349–1358
- 17 Escolano C, Amat M, Bosch J. *Chem Eur J*, 2006, 12: 8198–8207
- 18 Vitaku E, Smith DT, Njardarson JT. *J Med Chem*, 2014, 57: 10257–10274
- 19 Jiang W, Li Y, Wang Z. *Chem Soc Rev*, 2013, 42: 6113–6127
- 20 Kukhar VP and Soloshonok VA, ed. *Fluorine Containing Amino Acids—Synthesis and Properties*. Chichester: Wiley, 1995
- 21 Shimizu M, Hiyama T. *Angew Chem Int Ed*, 2005, 44: 214–231
- 22 Schlosser M. *Angew Chem Int Ed*, 2006, 45: 5432–5446
- 23 Uneyama K, Katagiri T, Amii H. *Acc Chem Res*, 2008, 41: 817–829
- 24 Smits R, Cadicamo CD, Burger K, Koksche B. *Chem Soc Rev*, 2008, 37: 1727–1739
- 25 Nie J, Guo HC, Cahard D, Ma JA. *Chem Rev*, 2010, 111: 455–529
- 26 Merino E, Nevado C. *Chem Soc Rev*, 2014, 43: 6598–6608
- 27 Ojima I, Macarthy JR, Welch JT. *Biomedical Frontiers of Fluorine Chemistry*. New York: American Chemical Society, 1996
- 28 Luzina EL, Popov AV. *J Fluorine Chem*, 2014, 168: 121–127
- 29 Kaur K, Kumar V, Gupta GK. *J Fluorine Chem*, 2015, 178: 306–326
- 30 Zanda M. *New J Chem*, 2004, 28: 1401–1411
- 31 Dmowski W. *Wiadomosci Chemiczne*, 1997, 51: 263–291
- 32 Tredwell M, Gouverneur V. Edited by Carreira EM, Yamamoto H. *Fluorine in medicinal chemistry: Importance of chirality*. *Compre Chiral*, 2012, 1: 70–85
- 33 Huisgen R. *Angew Chem Int Ed*, 1963, 2: 565–598
- 34 Padwa A and Pearson WH. *Synthetic Applications of 1,3-Dipolar Cycloaddition Chemistry Toward Heterocycles and Natural Products*. New York: Wiley-VCH, 2002
- 35 Hashimoto T, Maruoka K. *Chem Rev*, 2015, 115: 5366–5412
- 36 Adrio J, Carretero JC. *Chem Commun*, 2019, 55: 11979–11991
- 37 Wei L, Chang X, Wang CJ. *Acc Chem Res*, 2020, 53: 1084–1100
- 38 Zhao P, Li Z, He J, Liu X, Feng X. *Sci China Chem*, 2021, 64: 1355–1360
- 39 Li YN, Chang X, Xiong Q, Dong XQ, Wang CJ. *Chin Chem Lett*, 2021, 32: 4029–4032
- 40 Stohler R, Wahl F, Pfaltz A. *Synthesis*, 2005, 2005: 1431–1436
- 41 Chen XH, Wei Q, Luo SW, Xiao H, Gong LZ. *J Am Chem Soc*, 2009, 131: 13819–13825
- 42 Cristóbal C, Gaviña D, Alonso I, Ribagorda M, Carretero JC, del Pozo C, Adrio J. *Chem Commun*, 2022, 58: 7805–7808
- 43 Deng Y, Dong Z, Gao F, Guo Y, Sun M, Li Y, Wang Y, Chen Q, Wang K, Yan W. *J Org Chem*, 2021, 86: 13011–13024
- 44 Feng B, Lu LQ, Chen JR, Feng G, He BQ, Lu B, Xiao WJ. *Angew Chem Int Ed*, 2018, 57: 5888–5892
- 45 Shen C, Yang Y, Wei L, Dong WW, Chung LW, Wang CJ. *iScience*, 2019, 11: 146–159
- 46 Xu S, Zhang ZM, Xu B, Liu B, Liu Y, Zhang J. *J Am Chem Soc*, 2018, 140: 2272–2283
- 47 Gill M, Das A, Singh VK. *Org Lett*, 2022, 24: 5629–5634
- 48 Li QH, Tong MC, Li J, Tao HY, Wang CJ. *Chem Commun*, 2011, 47: 11110–11112
- 49 Li QH, Xue ZY, Tao HY, Wang CJ. *Tetrahedron Lett*, 2012, 53: 3650–3653
- 50 López-Pérez A, Adrio J, Carretero J. *Angew Chem Int Ed*, 2009, 48: 340–343
- 51 Tong MC, Li J, Tao HY, Li YX, Wang CJ. *Chem Eur J*, 2011, 17: 12922–12927
- 52 Chang X, Yang Y, Shen C, Xue KS, Wang ZF, Cong H, Tao HY, Chung LW, Wang CJ. *J Am Chem Soc*, 2021, 143: 3519–3535
- 53 See computational details in the Supplementary Information
- 54 Lam Y, Grayson MN, Holland MC, Simon A, Houk KN. *Acc Chem Res*, 2016, 49: 750–762
- 55 Peng Q, Paton RS. *Acc Chem Res*, 2016, 49: 1042–1051
- 56 Tantillo DJ. *Acc Chem Res*, 2016, 49: 741–749
- 57 Ahn S, Hong M, Sundararajan M, Ess DH, Baik MH. *Chem Rev*, 2019, 119: 6509–6560
- 58 Harvey JN, Himo F, Maseras F, Perrin L. *ACS Catal*, 2019, 9: 6803–6813
- 59 Lan J, Li X, Yang Y, Zhang X, Chung LW. *Acc Chem Res*, 2022, 55: 1109–1123
- 60 Ess DH, Houk KN. *J Am Chem Soc*, 2008, 130: 10187–10198
- 61 Wang M, Wang CJ, Lin Z. *Organometallics*, 2012, 31: 7870–7876
- 62 Pascual-Escudero A, de Cózar A, Cossío FP, Adrio J, Carretero JC. *Angew Chem Int Ed*, 2016, 55: 15334–15338
- 63 Domingo LR, Ríos-Gutiérrez M, Pérez P. *J Org Chem*, 2018, 83: 10959–10973
- 64 Cheng F, Kalita SJ, Zhao Z, Yang X, Zhao Y, Schneider U, Shibata N, Huang Y. *Angew Chem Int Ed*, 2019, 58: 16637–16643
- 65 Xiong Y, Du Z, Chen H, Yang Z, Tan Q, Zhang C, Zhu L, Lan Y, Zhang M. *J Am Chem Soc*, 2019, 141: 961–971
- 66 Li B, Xu H, Dang Y, Houk KN. *J Am Chem Soc*, 2022, 144: 1971–1985
- 67 Chang X, Liu XT, Li F, Yang Y, Chung LW, Wang CJ. *Chem Sci*, 2023, 14: 5460–5469
- 68 Xu L, Chung LW, Wu YD. *ACS Catal*, 2016, 6: 483–493
- 69 Gao W, Lv H, Zhang T, Yang Y, Chung LW, Wu YD, Zhang X. *Chem Sci*, 2017, 8: 6419–6422
- 70 Lan J, Liao T, Zhang T, Chung LW. *Inorg Chem*, 2017, 56: 6809–6819
- 71 Zhang X, Chung LW. *Chem Eur J*, 2017, 23: 3623–3630
- 72 Wu SB, Zhang T, Chung LW, Wu YD. *Org Lett*, 2019, 21: 360–364
- 73 Yang Y, Zhang X, Zhong LP, Lan J, Li X, Li CC, Chung LW. *Nat Commun*, 2020, 11: 1850
- 74 Du X, Xiao Y, Yang Y, Duan Y, Li F, Hu Q, Chung LW, Chen G, Zhang X. *Angew Chem Int Ed*, 2021, 60: 11384–11390
- 75 Lan J, Zhang T, Yang Y, Li X, Chung LW. *Inorg Chem*, 2022, 61: 18019–18032
- 76 Morokuma K. *Acc Chem Res*, 1977, 10: 294–300
- 77 Ess DH, Houk KN. *J Am Chem Soc*, 2007, 129: 10646–10647
- 78 Bickelhaupt FM, Houk KN. *Angew Chem Int Ed*, 2017, 56: 10070–10086
- 79 Chen C, Zhang Z, Jin S, Fan X, Geng M, Zhou Y, Wen S, Wang X, Chung LW, Dong XQ, Zhang X. *Angew Chem Int Ed*, 2017, 56: 6808–6812
- 80 Kalita SJ, Zhao Z, Li Z, Cheng F, Zhao Y, Huang Y. *Eur J Org Chem*, 2021, 2021(40): 5530–5535
- 81 Calvo JS, Villones RLE, York NJ, Stefaniak E, Hamilton GE, Stelling AL, Bal W, Pierce BS, Meloni G. *J Am Chem Soc*, 2022, 144: 709–722
- 82 Mooibroek TJ, Aromí G, Quesada M, Roubeau O, Gamez P, DeBeer George S, van Slageren J, Yasin S, Ruiz E, Reedijk J. *Inorg Chem*, 2009, 48: 10643–10651
- 83 Castañeda-Arriaga R, Pérez-González A, Alvarez-Idaboy JR, Galano A. *Int J Quantum Chem*, 2018, 118: e25527